Hindawi
International Transactions on Electrical Energy Systems
Volume 2023, Article ID 3708751, 15 pages
https://doi.org/10.1155/2023/3708751

Research Article

Performance Analysis of Bus Voltage in Distribution Network with High Penetration of PV Controlled via Data-Driven Approach

Anju Yadav,[1] **Nand Kishor**,[2] **Richa Negi**,[1] **Mikael Opas**,[3] **and Petra Raussi**[3]

[1]*Department of Electrical Engineering, Motilal Nehru National Institute of Technology, Allahabad, India*
[2]*Østfold University College, Fredrikstad Campus, Fredrikstad, Norway*
[3]*Smart Grids, VTT Technical Research Centre, Espoo, Finland*

Correspondence should be addressed to Nand Kishor; nand_research@yahoo.co.in

Received 26 May 2023; Revised 30 August 2023; Accepted 19 September 2023; Published 30 September 2023

Academic Editor: Silvio Giuseppe Di Santo

Integration of large-scale distributed photovoltaic (PV) generation resources can lead to technical challenges, particularly voltage rise caused by PVs power injection at the time of high solar radiation profile and low load demand. Reactive power control of PV inverters can help mitigate the voltage rise, which arises just for a short duration due to high incident solar radiation. There is a possibility to control functions on these PV inverters based on the rating of the PV inverter. For one-second resolution, local data-driven voltage sensitivity estimation is applied to update the control functions such as volt-var and volt-watt on the PV inverters so as to regulate the bus voltage. Different forms of solar radiation profiles, transient varying, smooth varying, and worst operating scenario corresponding to the minimum load at the time of high PV generation, are included. The study is demonstrated for different PV penetration levels. The voltage analysis on buses is performed using power hardware (PV emulator) in the loop simulation, at one of the buses in the network, while the remaining PVs are being controlled using volt-var control (VVC)/volt-watt control (VWC) methods. The applied approach confirms to maintaining bus voltage within limits even against a very short transient time instant of solar radiation profile.

1. Introduction

The voltage regulation in the distribution network (DN) has been addressed at different time scales: centralized, decentralized, and distributed level control. The voltage regulation formulated as an optimization problem [1] requires full information about the network and has greater computation and communication requirements. They are usually operated at longer (e.g., 15 min) dispatch intervals. On the other hand, in decentralized control, the set points of smart inverters are established via communication among the neighboring inverters in [2]. However, there exists a high level of uncertainty and plug-and-play ability of distributed generation resources, so the system conditions can change rapidly. As a result, decentralized control alone cannot sufficiently address the voltage regulation issue [3]. In some situations, bus voltages may still violate the operation limits even with the prespecified droop settings and dispatch set points. An optimal sizing and siting problem of DGs is presented in [4] to minimize the voltage drops and total power losses. The optimization problem is solved using the Harris Hawks optimizer (HHO) by considering different seasonal load conditions.

Similarly, in distributed control, the P/V [5] and Q/V characteristic (curves) [6] strategies are implemented using only local measurements. It is agreed that predefined rules for framing these characteristics have resulted in stable performance and fast convergence, but their equilibria unfortunately do not coincide with the desired optimized power flow conditions [7]. In [8], author presents local piecewise linear droop functions as constraints for volt-var control (VVC)/volt-watt control (VWC) capabilities for PV, considering mixed-integer linear programming problem in an unbalanced distribution grid optimal power flow (DOPF) model. For that, the authors adopt the LinDist3Flow version of DOPF and perform a simulation on an IEEE 123-node

feeder with 15 utility-scale PV and battery energy storage system inverters to validate the proposed approach for effective voltage regulation and control. A distributed control scheme remains effective, due to the use of local information when compared to a centralized control scheme, which may fail on the occurrence of latency in communication. As such, local control schemes cannot guarantee optimal performance. This makes real-time coordination among local controllers necessary.

1.1. Related Work Reviews. The comparison among different types of PV inverter control strategies and dispatch approaches based on voltage sensitivity, a centralized controller, and the local voltage measurement is presented in [9]. The control system resiliency can be increased by being dependent on the local voltage control, especially when the communication-based distributed control fails. This evolves into a hierarchical or multilevel control scheme, a two-stage control scheme using local droop control and distributed control [3]. In [10], a convex formulation for optimal sizing and siting is presented for PV and battery energy storage system. An optimal control of grid-tied PV integrated microgrid under partially shaded conditions is presented in [11]. All control algorithms are implemented in a DSpace 1104 environment and largely tested under various partially shaded patterns. Most of the design strategies discussed in the available literature fail to provide generalized selection criteria for control parameter settings. The presence of multiple PV inverters, each trying to control their local voltage, may lead to oscillation [12]. In other words, undesired potential interactions arise among the PV inverters and DN impedance.

In [13], authors have reported volt-watt and volt-var based on voltage sensitivity. A regression model was developed to determine the voltage sensitivity, with voltage variations against active power changes. However, to mention, the capacity of PV inverters remains under study. In other words, the volt-watt characteristic of all PV inverters, including at the feeder end, is the same. As such, volt-watt function can be conveniently adjusted, based on its location from the grid connection so as to limit the voltage violation. Thus, analytically derived rules may indicate stable performance, but they are difficult to implement in a system with PV inverters of different capacities. Recently, in the study [14], a direct power control method was proposed for grid-integrated PV inverters at point of common coupling (PCC) so that the active and reactive power flow can be regulated directly between the microgrid and utility grid by controlling the PCC voltage. In [15], authors have used genetic algorithms to observe the optimization solution approach in the smart grid to maintain power quality and availability. This paper also presented the critical factors of nonconventional energy resources for managing the energy and forecasting the load.

1.2. Scope for Study. A well-known issue also discussed later in the manuscript is voltage violations, particularly at feeder end buses, even with PV integration. In addition, the transient solar radiation profile can lead to increased voltage variability across the network. During the period of transiently varying solar radiation profiles, the DN is subjected to serious variation in the bus voltage profile. As such, traditional voltage regulators need 30–60 seconds to change the tap that may not be suitable to compensate for rapidly varying voltage changes. Using PV inverters at a fixed inductive power factor (absorb reactive power) can alleviate the over-voltage, but it is effective only when local PV generation becomes more than demand. This situation is foreseen at the time of high PV power generation, with solar radiation at its peak. However, during the day, the voltage drop can also be seen at the time of high demand and low solar radiation availability.

1.3. Motivation and Contributions. The low-voltage DN is usually unbalanced and has both single- and three-phase loads connected. Due to unevenly distributed single-phase loads and asymmetrical line impedances, the prevailing voltage unbalance may lead to increased network losses and even instability in the system [16]. Existing voltage regulation is not capable of solving the phase unbalance issue that arises in single-phase and three-phase PV installation in the network. During mid-day operation, when output power from the inverter increases, thus, available reactive power capacity reduces. As a result, suppression of voltage rise is limited. Furthermore, due to changes in topology reconfiguration, it would be a difficult task to work with an accurate model.

A review on the challenges and objectives of data-driven smart building-integrated PV systems is presented in [17]. As such, data-driven methods can be viable options. With smart data availability, 15–30 min data sampled at a rate of 1 data per sec can be used to develop a regression model between measured bus voltages and power (active/reactive) injection to estimate the voltage sensitivity factors. In order to accurately estimate the sensitivities, a huge amount of data is required, but the method needs to be developed without having a need for huge data. A linear model that approximates the nonlinear relationship between the voltage magnitudes and power injections, to estimate the voltage sensitivities, based on a data-driven approach can be found in [18]. The recursive technique can be applied to estimate the sensitivity of bus voltage and power loss in an unbalanced DN, having PV integration. Thus, sensitivity coefficients can be updated for any variations in network operating conditions. Subsequently, volt-var control (VVC)/volt-watt control (VWC) can be modified for the control of PV inverters towards voltage regulation.

The motivation of this work is to assess the voltage rise caused by PV power injection at the time of high solar radiation profiles and low load demand. Advanced controls like VVC/VWC could allow the PV inverters to gradually reduce their real power output as a function of measured bus voltage and provide reactive power support to maintain the network voltage within constraints. Therefore, the author's objective is to assess bus voltage status under PV power generation with solar radiation of (i) transient varying,

(ii) short-surge, and (iii) smooth peak characteristics. Further, the proposed approach updates the VVC/VWC algorithms, according to data-driven voltage sensitivity estimation so as to achieve voltage within limits. Next, apply the proposed control design on a real-time simulator. The focus is to understand any interaction between PV inverters modeled in RTDS controlled via VVC/VWC and power injection via a PV emulator (droop-controlled) at one of the buses in the network towards voltage regulation. The present study is carried out on an unbalanced IEEE-13 bus DN, which has nonuniformity in the distribution of loads throughout the phases and buses. The planning of PV placement is based on optimal locations of three-phase nodes at feeder buses [19] and subsequently applies the VVC/VWC method to analyze the PV power, while maintaining voltage limits within the network. During this stage, voltage analysis is performed to check the variation in voltage, mainly at feeder end buses with PVs system.

This paper is organized as follows. Section 2 describes the modeling of the network and the use of the simulation platform. Section 3 presents bus voltage analysis for control design implemented using OpenDSS and MATLAB (GridPV toolbox). Section 4 presents the discussions on bus power and voltage for results obtained from real-time simulation with the injection of power from grid emulators. Section 5 concludes the work.

2. Distribution Network Modeling and Simulation Platform

In the study, an unbalanced DN (IEEE-13 bus network) is considered with load and PV installation at buses 634 and 671. Bus 634, 671, and 680 are referred to as near (*N*), mid (*M*), and far-away (*F*) locations, as shown in Figure 1. All these buses have base loads, as referred to in [20]. The 3-phase PVs are placed on these buses (each of 0.4125 MW). Next, Figure 2 represents the solar radiation profiles, where the solar profile illustrated in Figure 2(a) is used in analysis on the simulation platform, while the one shown in Figure 2(b) is used in the study on a real-time simulation platform. The transient varying solar radiation is sampled at a rate of one data per 2 sec, while smooth varying is an hourly sample data.

2.1. MATLAB and OpenDSS Interface Simulation. In this part of the simulation platform, the open-source distribution system software (OpenDSS) and GridPV toolbox developed by the Electric Power Research Institute and SANDIA National Laboratories, respectively, have been used. In OpenDSS, a 3-phase DN load flow analysis can be solved, including unbalanced phases, DGs integration, and future smart grid applications [21]. The GridPV toolbox [22] is run on the MATLAB platform. Using these tools, the DN and solar PV systems can be easily modeled. They also support the simulation of a high-resolution time-series power flow analysis, particularly against solar radiation. The complete modeling and analysis with the integration of OpenDSS and MATLAB (GridPV) are provided through a COM server

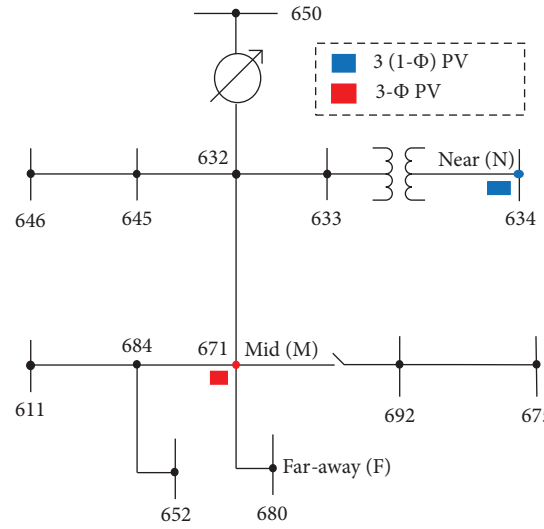

Figure 1: IEEE-13 bus DN.

interface. In the GridPV toolbox, the wavelet variability model [21] is applied to convert solar radiation data, smoothening the variability to compute PV system size and density in the given area. Next, the VVC and VWC approaches discussed in the next section are applied to the PV inverters.

Figure 3 illustrates the interface of two simulation platforms [23] for voltage profile analysis. With the selected PV placement and its size (MW), the information is stored in a .mat file to be added to the OpenDSS platform, which creates a .dss file. The given PV system data and the solar radiation data are created in both the .txt file and the .dss file for objects in OpenDSS. The GridPV toolbox initializes the COM interface in MATLAB to communicate with the OpenDSS in loading and compiling DNs (circuits) for analysis. Now, time-series analysis is performed in OpenDSS to understand the impact of the variability of solar radiation and PV placement on the voltage profile, as discussed in the next section.

2.2. Real-Time Simulation Testbed. As shown in Figure 4, DN (IEEE-13 bus network) with placement and size of PV inverter (in RTDS) will be controllable via updated VVC and VWC on PV inverters. All the communications required for the distributed control algorithm (applied to three single-phase PV inverters in RTDS) are implemented via a real communication network with the IEC 61850 protocol. Note in said figure that power hardware (PV emulator), which is droop-controlled is also used to inject power into one of the buses. The bus (having PV integrated) signal (in RTDS) is retrieved independently and routed through the communication card to the control algorithm (in PC) and subsequently designed control signal is transmitted back to the PV inverter (in RTDS). The results obtained from RTDS are stored in a DAT file. The DAT file is a data file that contains information about the result, which has been stored and further analyzed. The DAT file can be accessed using RSCAD, MATLAB, and any text editor like notepad.

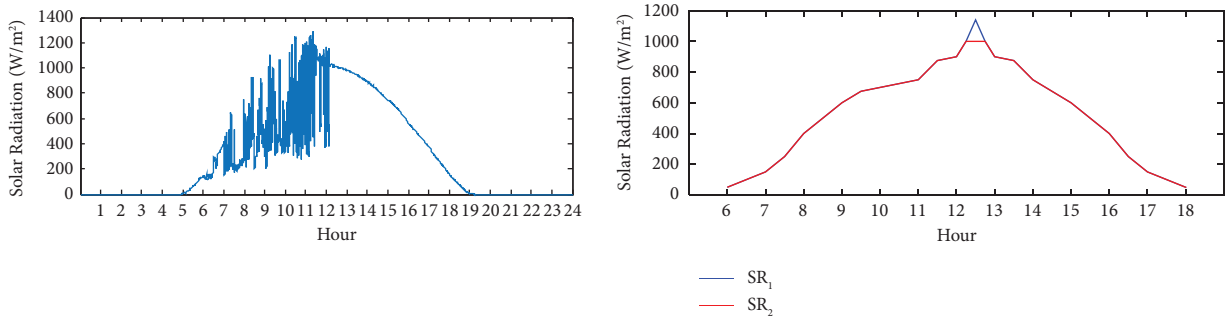

Figure 2: Solar radiation profiles. (a) Transient varying. (b) Smooth varying.

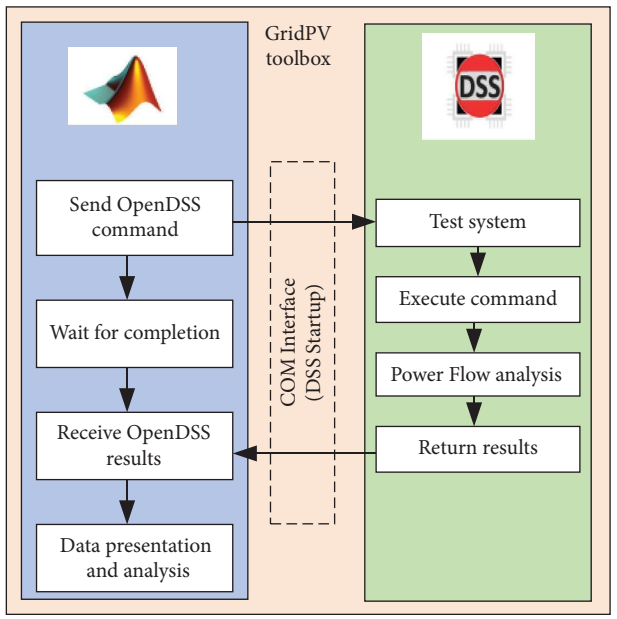

Figure 3: Workflow for the MATLAB-openDSS interface.

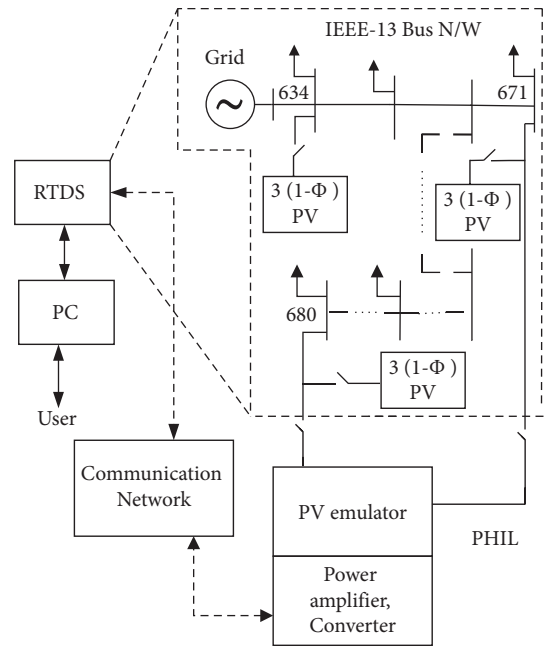

Figure 4: Integration of components in hardware setup.

3. Data-Driven Control Parameter

This section discusses the algorithm applied to modulate the active/reactive power in PV inverters so as to update the VVC/VWC-based voltage sensitivity coefficient estimation for a range of data sample. Considering the DN belongs to a community-scaled area, identical PV and load profiles can be applied to each bus. With smart data availability, 15–30 min data, sampled at a rate of one data point per sec can be used to develop the regression model between measured bus voltages and power (active/reactive) injection to estimate the voltage sensitivity factors.

With linearization around network operating conditions, the reactive power index can be defined as the sensitivity of voltage deviation with respect to per unit change in the reactive power of the PV inverter and can be written in the matrix form as follows:

$$\Delta Q(t) = \left[\Delta v_1(t)\Delta v_2(t)\ldots\Delta v_{N_i}(t)\right]\bullet\left[S_{\mathrm{VQ}}\right], \quad (1)$$

where $\Delta v_{N_i}(t) = v_{N_i} - v_R(t)$ and $S_{\mathrm{VQ}} = \partial V/\partial Q$ as a voltage sensitivity matrix with respect to reactive power injection (V-Q).

Similarly, the active power index can be defined as the sensitivity of voltage deviation with respect to per unit change in the active power of the PV inverter and can be written in the matrix form as follows:

$$\Delta P(t) = \left[\Delta v_1(t)\Delta v_2(t)\ldots\Delta v_{N_i}(t)\right]\bullet\left[S_{\mathrm{VP}}\right], \quad (2)$$

where $\Delta v_{N_i}(t) = v_{N_i}(t) - v_R(t)$ and $S_{\mathrm{VP}} = \partial V/\partial P$ as a voltage sensitivity matrix with respect to active power injection (V-P).

To note, voltage sensitivity matrices are functions of t, but their variations remain small for a wide range of operating conditions. The voltage magnitude of phase α at bus i with respect to injected active and reactive power of phase β at bus j is as follows:

$$\Delta V_i^{\alpha} \approx \sum_{j \in N_i} \sum_{\beta \in N_p} \rho_{ij}^{\alpha\beta} \Delta P_j^{\beta} + \mu_{ij}^{\alpha\beta} \Delta Q_j^{\beta}, \tag{3}$$

where $\rho_{ij}^{\alpha\beta}$ and $\mu_{ij}^{\alpha\beta}$ are, respectively, V-P and V-Q sensitivity coefficients, i.e., $\rho_{ij}^{\alpha\beta} \in \Lambda_{ij}$ and $\mu_{ij}^{\alpha\beta} \in \Pi_{ij}$.

From the measurement data of change in voltage, active power, and reactive power, now it is required to estimate the sensitivity coefficients, with (3) written in the following form:

$$[\Delta V] = \begin{bmatrix} S_{VP} & S_{VQ} \end{bmatrix} \begin{bmatrix} \Delta P \\ \Delta Q \end{bmatrix} + \epsilon(k). \tag{4}$$

Figure 5 illustrates the flowchart for estimation of voltage sensitivity estimation carried out for every window of data sample of power-flow analysis.

Equation (4) can be rewritten for a given data sample k for window length as follows:

$$\mathbf{Y} = [\mathbf{X}_S]\Psi, \tag{5}$$

where

$$\begin{aligned} \mathbf{Y} &= \left[\mathbf{y}_1^{N_P}(k) \mathbf{y}_2^{N_P}(k) \mathbf{y}_3^{N_P}(k), \ldots, \mathbf{y}_{N_i}^{N_P}(k) \right]^{\mathbf{T}}, \\ \Psi &= \left[\boldsymbol{\phi}_1^{N_P}(k) \boldsymbol{\phi}_2^{N_P}(k) \boldsymbol{\phi}_3^{N_P}(k_3), \ldots, \boldsymbol{\phi}_{N_i}^{N_P}(k) \right]^{\mathbf{T}}. \end{aligned} \tag{6}$$

$\mathbf{X}_S$ is the unknown matrix, representing the sensitivity coefficients, to be determined. $\mathbf{y}_{N_i}^{N_P}(k)$ is a column vector of measured voltage magnitude change of phase N_p at bus i, and $\phi_{N_i}^{N_P}(k)$ is a column vector of measured change in active power and reactive power of phase N_p at bus i at discrete time instant k.

From (5), the information matrix Ω can be written upto data samples s as follows:

$$\Omega = \sum_{k=1}^{s} \boldsymbol{\phi}_{N_i}^{N_P}(k) \left[\boldsymbol{\phi}_{N_i}^{N_P} \right]^T (k) = \Psi^T \Psi. \tag{7}$$

In the next step, the matrix can be estimated with objective function defined as follows:

$$J\left(\widehat{\mathbf{X}_S}, s\right) = \left\| \mathbf{Y} - \Psi \widehat{\mathbf{X}_S} \right\|_2^2, \tag{8}$$

where $\left\| \mathbf{Y} - \Psi \widehat{\mathbf{X}_S} \right\|_2^2$ represents the Euclidean norm.

In the proposed study, the sensitivity matrix can be estimated using [24]. From the estimated matrix, ΔP_j^{β} and ΔQ_j^{β} of phase β at bus j can be adjusted such that

$$V_{\min} \le \mathbf{V} + \mathbf{S}_{VP} \Delta \mathbf{P} + \mathbf{S}_{VQ} \Delta \mathbf{Q} \le V_{\max}, \tag{9a}$$

$$-\mathbf{Q_{min}} \le \mathbf{Q} \le \mathbf{Q_{max}}, \tag{9b}$$

where $\Delta \mathbf{P}$ is the vector control of active power, achievable via VWC for each PV inverter, and $\Delta \mathbf{Q}$ is vector control of reactive power to be absorbed or injected as per VVC by PV inverters.

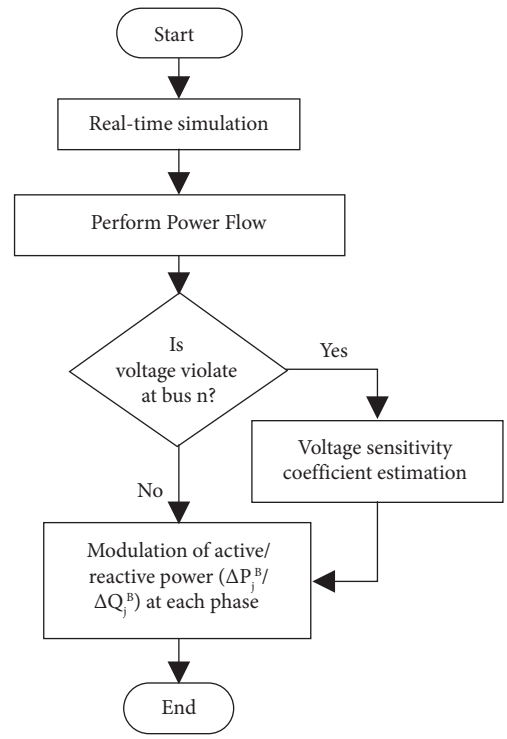

Figure 5: Flowchart of the power flow-based voltage sensitivity estimation.

Those buses, having voltage violations, or nearby PV inverters will be subjected to compensate required reactive power. As such from (3)–(9), the amount of modulation ΔQ_j^{β} required at PV inverter in phase β at bus j is given as follows:

$$\Delta Q_j^{\beta} = \begin{cases} \left[\mu_{ij}^{\alpha\beta} \right]^{-1} \times \left(v_{\min} + v_n - v \right)_{N_i}(k), \\ \left[\mu_{ij}^{\alpha\beta} \right]^{-1} \times \left(v_{\max} - v_m - v \right)_{N_i}(k), \end{cases} \tag{10}$$
$$\cdot \begin{cases} v < v_{\min}, & v_{\min} = 0.95, \quad v_n = 0.98, \\ v > v_{\max}, & v_{\max} = 1.05, \quad v_m = 1.02. \end{cases}$$

The voltage regulation will be performed by each PV inverter, depending upon its availability of reactive power compensation (preferred), while active power compensation (curtailment) will be set as auxiliary.

Active power supply from these PV inverters involved in reactive power compensation is given by

$$\Delta P_{c,j}^{\beta} = \sqrt{\left(S_j^{\beta} \right)^2 - \left(Q_j^{\beta} + \Delta Q_j^{\beta} \right)^2}. \tag{11}$$

Thus, if the capacity of reactive power compensation is insufficient in the complete network, then those PV inverters having least voltage sensitivity with respect to active power (i.e., larger capacity PV inverter) will be considered for curtailment. The amount of modulation ΔP_j^{β} required at PV inverter in phase β at bus j is given as follows:

$$\Delta P_j^{\beta} = \left[\rho_{ij}^{\alpha\beta}\right]^{-1} \times \left(v - v_{\max}\right)_{N_i}(k). \quad (12)$$

The VVC and VWC are shown in Figure 6. Each of the PV inverters (of the same capacity) will be considered as an independent control variable in the decision-making. The control parameters of VVC can be considered as variables, according to the capacity of each PV inverter. Such inverters have a wide range of slopes to be defined (determined) between the smallest and largest capacity of PV inverters integrated in the network.

Thus, sensitivity coefficients can be updated for any variations in network operating condition. Subsequently, VVC and VWC can be modified for the control of PV inverters towards voltage regulation.

4. Voltage Analysis Using the Simulation Platform

Here, a total 1.2 MW (35%) capacity of PV is placed on buses 634, 671, and 680. The PV power output depends on the input solar radiation profile (Figure 2(a)), sampled at every 2 sec, which varies transiently in the first half. In the study, buses 671 and 680 are considered to include time-varying loads from their base load value. The two different random load curves such as LC_1 and LC_2 representing the summer and winter months [25], respectively, are shown in Figure 7, and it can be observed that the average load for a summer day is less as compared to a winter day. Also, to note, these load curves do not share symmetric time variation with PV output, which is in turn dependent on time-varying solar radiation.

In [26], authors have discussed semidefinite programming- (SDP)-based optimal power flow, and its numerical stability has been found to be very close to OpenDSS power flow results. This forms a basis to conclude that power flow calculations (solutions) from the theoretical approach (SDP optimal power), and those from OpenDSS are close to each other. As such, comparison of sensitivities calculation is discussed here. The power flow solution (without PV integration) for varying load LC_2 is obtained, and sensitivities are calculated at bus 634. At the said bus, phase C has the highest demand, while phase B has the lowest, so that the voltage of phase B remains higher and lower in phase C. As a result, the calculated sensitivities remain highest for phase B and lowest in phase C, as illustrated in Figure 8(a). However, the sensitivities calculated using OpenDSS become higher in phase A/phase B/phase C at some time instants; i.e., 2, 3, 13, and 14 hr, because corresponding phase voltage did not change (increase) with a decrease in grid power, as observed in Figure 8(b). From this, it can be concluded that the estimated sensitivities using OpenDSS are approximately equal to those obtained from SDP-based power flow solutions.

4.1. Bus Voltage at 35% PV Integration. Following the discussion from Section 3 on voltage sensitivity estimation according to the given range of data samples after performing a power flow solution, modulated power is applied based on the VVC/VWC characteristics of PV inverters. In the study, with a window length of every 2 min data (transient input solar radiation of 1 sample every 2 sec), output PV power, reactive power, and bus voltage are noted to estimate the voltage sensitivity coefficients.

With 35% PV integration, estimated voltage coefficients using signals from near (*N*) and mid (*M*) buses in the network are shown in Figure 9. The power at these nodes varies not only due to time-varying load but also fluctuations in PV generation. As a result, the buses experience a strong magnitude of power change. However, as observed in Figure 9(a), the voltage sensitivity with respect to active power change S_{VP} during the transient solar radiation period remains very low. On the other hand, in Figure 9(b), the voltage sensitivity against reactive power change S_{VQ} during the said period is significant, mainly at bus 634, i.e., *N* bus in the network. In other words, the bus near the grid is more voltage sensitive to changes in reactive power.

The variation of bus voltage in the network against the time-varying load curve LC_1 is shown in Figure 10. The solar radiation profile used in the GridPV toolbox is transient, and hence the fluctuations can be seen in the voltage profile on the buses, which have PV integration between 06:00 hrs to 12:00 hrs using both VVC and VWC for the PV inverter. The minimum and maximum voltage limits at every feeder bus are set as $V^{\min} = 0.95$ p.u. and $V^{\max} = 1.05$ p.u. Note that maximum transient is observed in phase C around 21:30 hrs at these buses when the largest change (surge) in load takes place. This suggests that controllers are capable of regulating the voltage against transient varying solar radiation (active power), but at least not so efficiently against load change. The voltage variation among the three phases is closer (balanced) at bus 634, as compared to bus 671. In addition, the voltage variation in phase B remains away from the unity value, while other phases, A and C, remain around the unity scale. The voltage profile, as shown in Figure 11, due to the impact of the time-varying load curve LC_2, is found to be comparatively more dynamic. It can be closely observed that due to the sudden jump in load at the time of reduced PV generation, the voltage dips instantaneously at 17:00 hrs. This fluctuation is prominent in phases A and C. With 35% PV integration, using both control methods, VVC and VWC, approximately similar voltage profile variations are obtained.

4.2. Bus Voltage at 50% and 100% PV Integration. To analyze the impact of higher PV generation power on feeder voltages, the PV integration in the network is increased. The PV capacity equivalent to 50% and 100% of the total load on buses 634 and 671 is introduced. The voltage profile after applying control is shown (for load curve LC_2), in Figure 12. As compared to the above integration amount (35%), the voltage variation (fluctuations) has an increasing trend with the addition of capacity, and this becomes significant for the mid (*M*) bus as compared to the *N* bus. In addition, variation in phase B voltage lies closer to the other two phases: A and C. The net active power and reactive power at these buses are shown in Figure 13. For 50% PV integration in Figure 13(a),

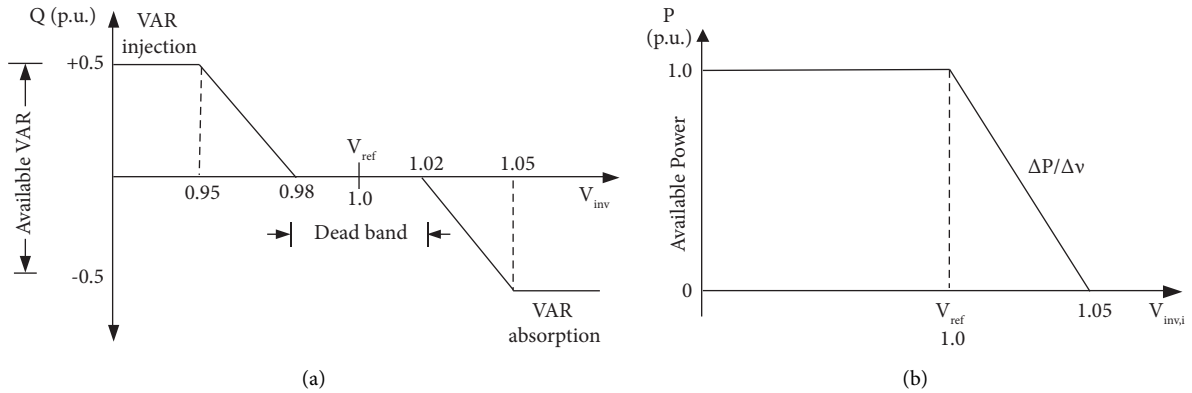

Figure 6: PV inverter control characteristics. (a) Volt-var characteristic (VVC). (b) Volt-watt characteristic (VWC).

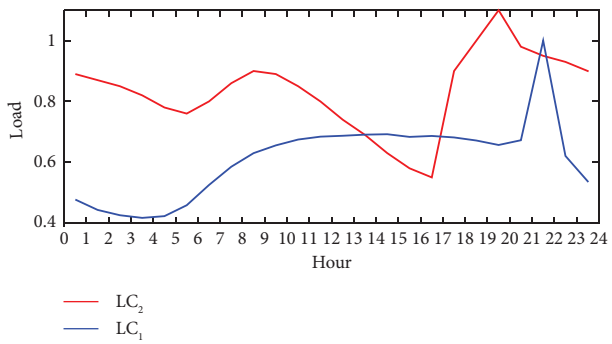

Figure 7: Different patterns of load curves.

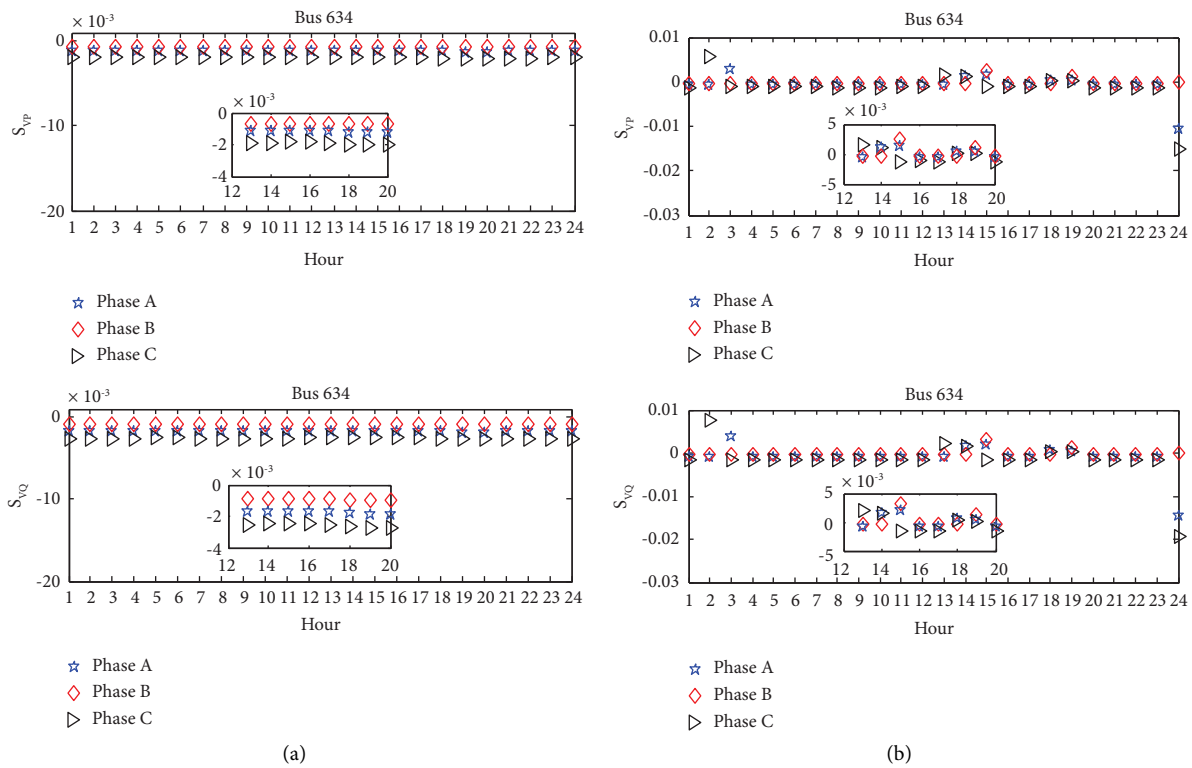

Figure 8: Sensitivities calculation for power flow solutions on load LC_2. (a) SDP-based power flow. (b) OpenDSS.

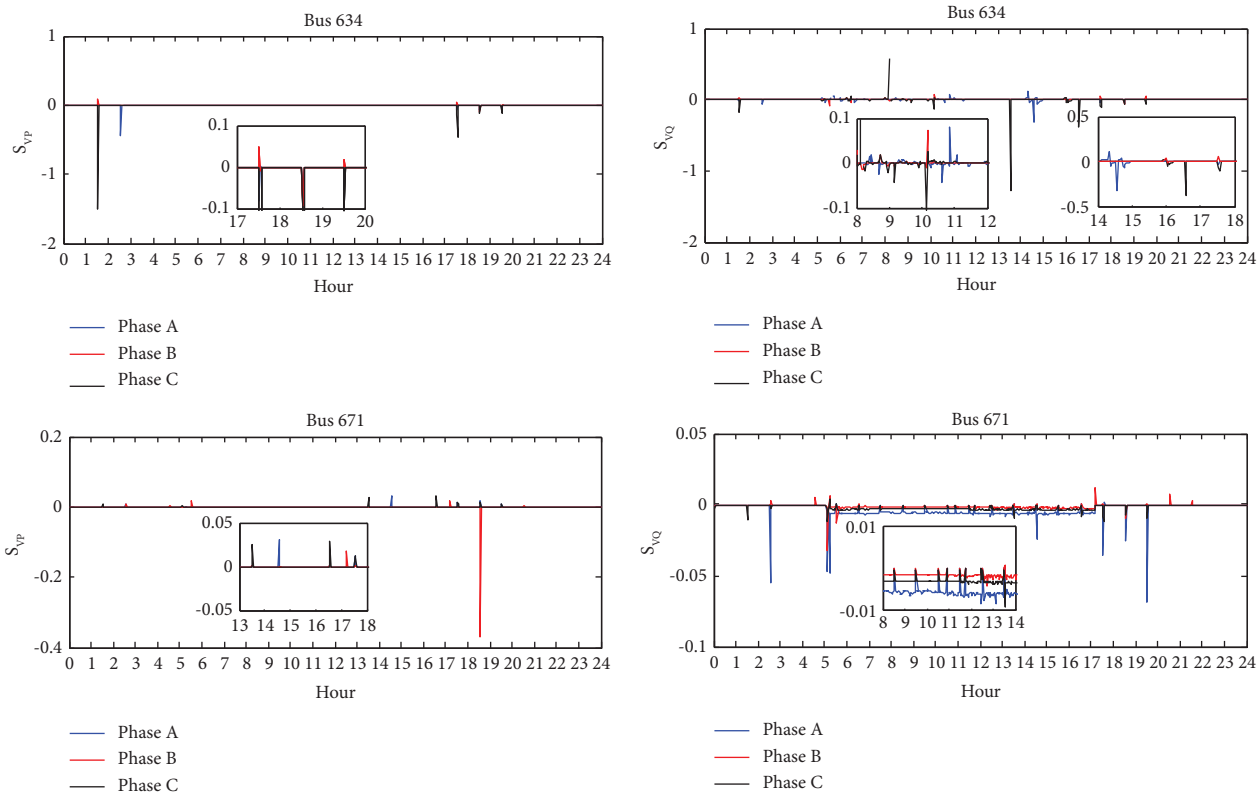

FIGURE 9: Voltage sensitivity after applying VVC control on PV inverters. (a) Voltage sensitivity with active power (S_{VP}). (b) Voltage sensitivity with reactive power (S_{VQ}).

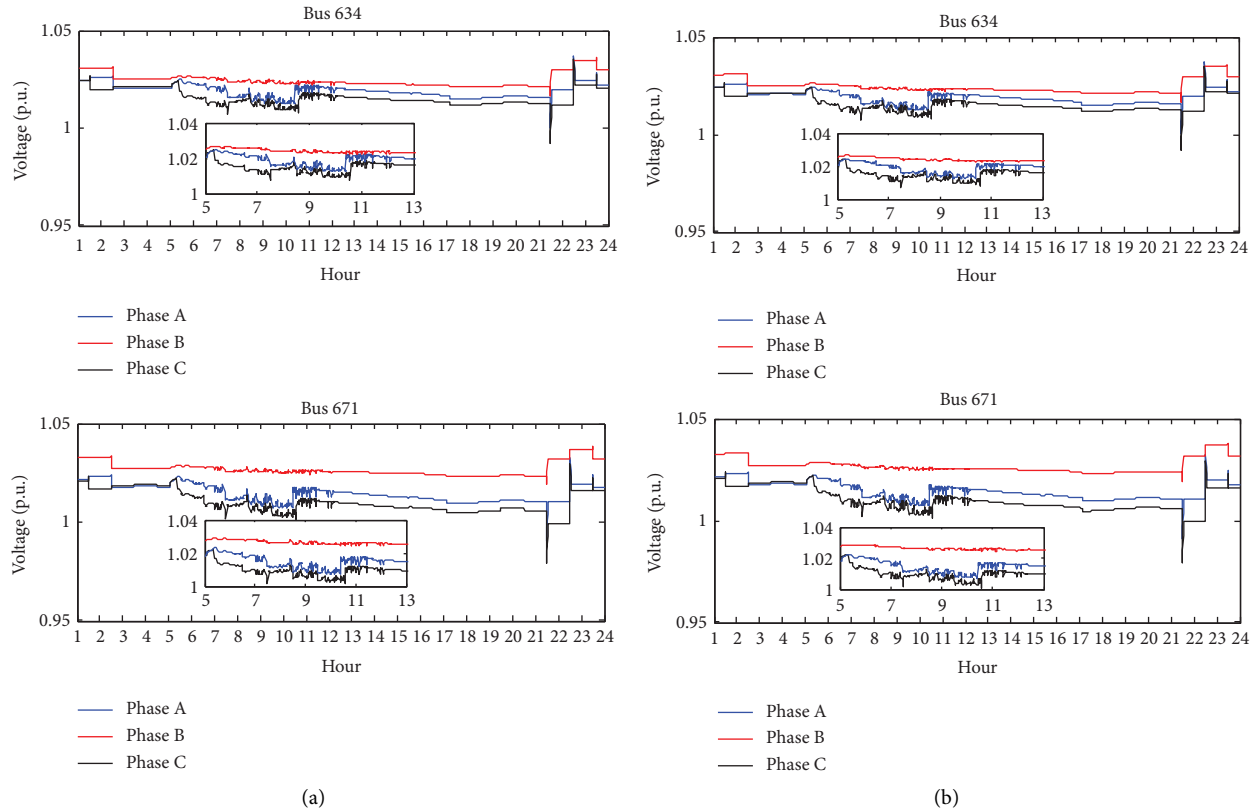

FIGURE 10: Voltage profile at 35% PV integration for LC_1. (a) VVC. (b) VWC.

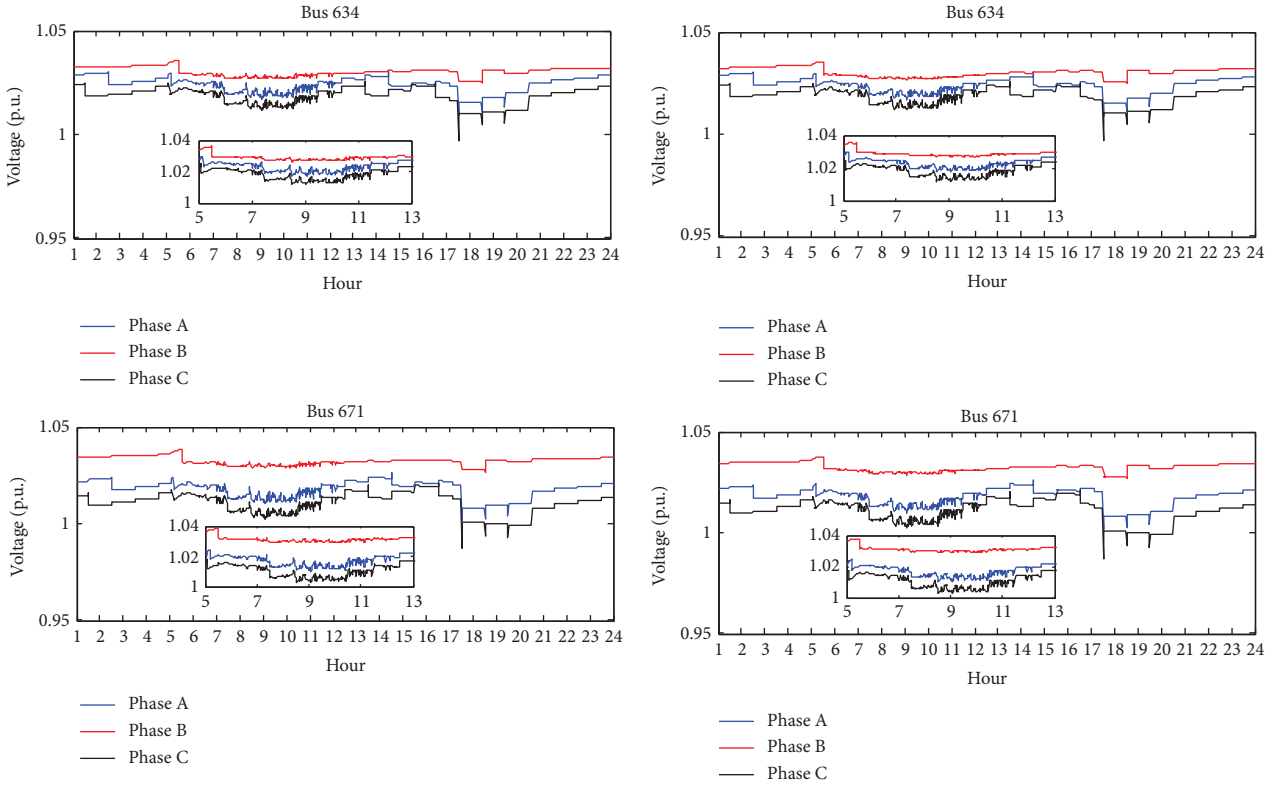

Figure 11: Voltage profile at 35% PV integration for LC_2. (a) VVC. (b) VWC.

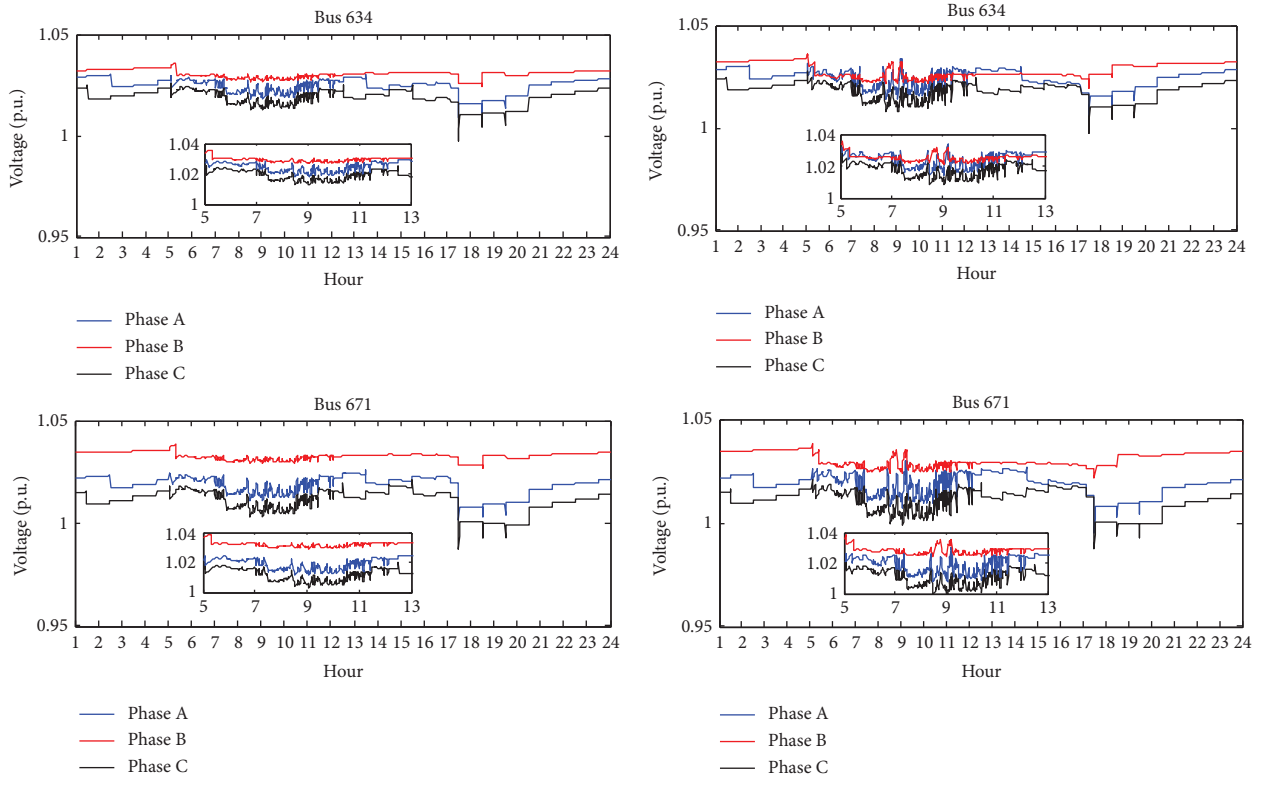

Figure 12: Voltage profile using proposed VVC control on PV inverters. (a) 50% PV integration. (b) 100% PV integration.

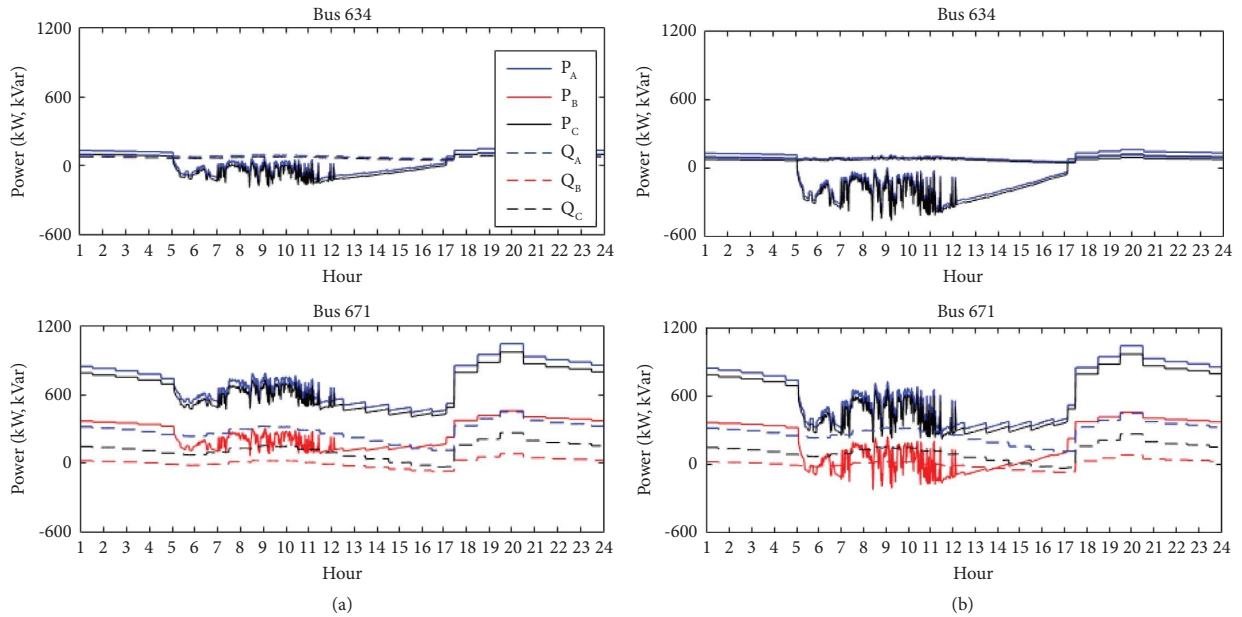

Figure 13: Power profile using proposed VVC control on PV inverters. (a) 50% PV integration. (b) 100% PV integration.

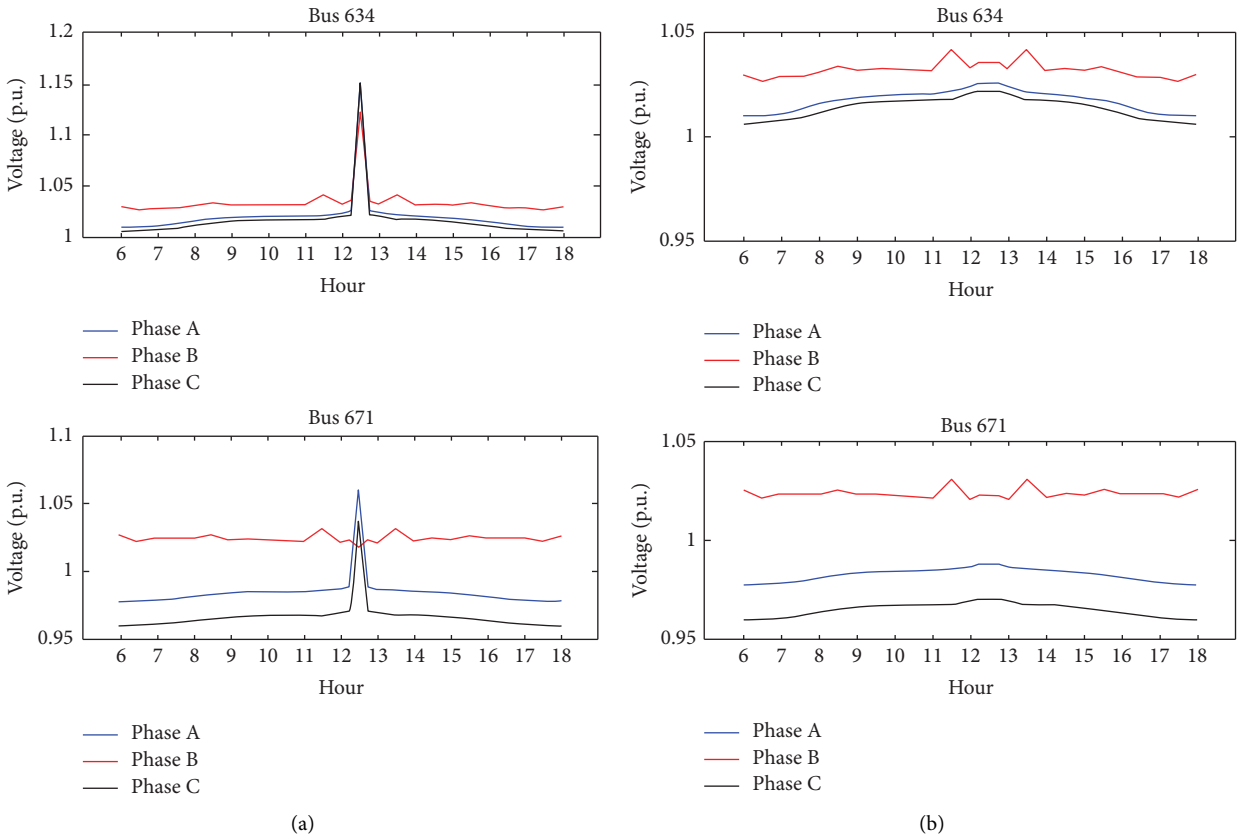

Figure 14: Bus voltages and PVs power without control on PV inverters (a) with solar radiation-1 (SR_1) and (b) with solar radiation-2 (SR_2).

power at bus 671 is regulated between 05 :00 hrs and 19: 00 hrs, and reactive power flow in three phases is adjusted in accordance to available net active power (amount). On the other hand, at bus 634, there is no reactive power support. Similarly, with increased PV penetration (100%) as illustrated in Figure 13(b), active power flow in phases A and C increases, which is obvious, but the trend in reactive power support remains like 50% PV integration. However, the effect of increased PV integration can be observed in the net active power corresponding to phase B.

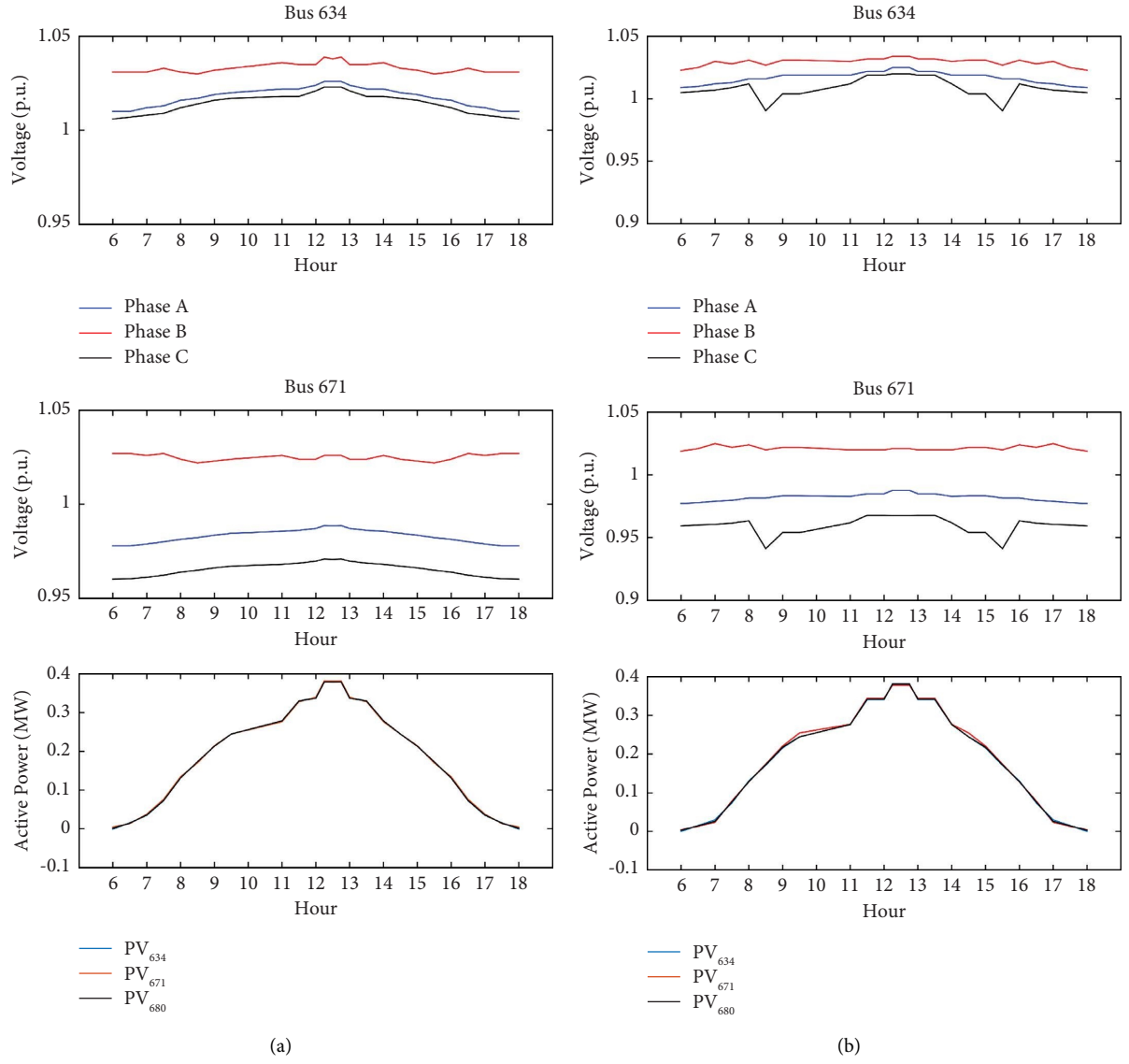

Figure 15: Bus voltages and PVs power with control on PV inverters at base load. (a) VVC control. (b) VWC control.

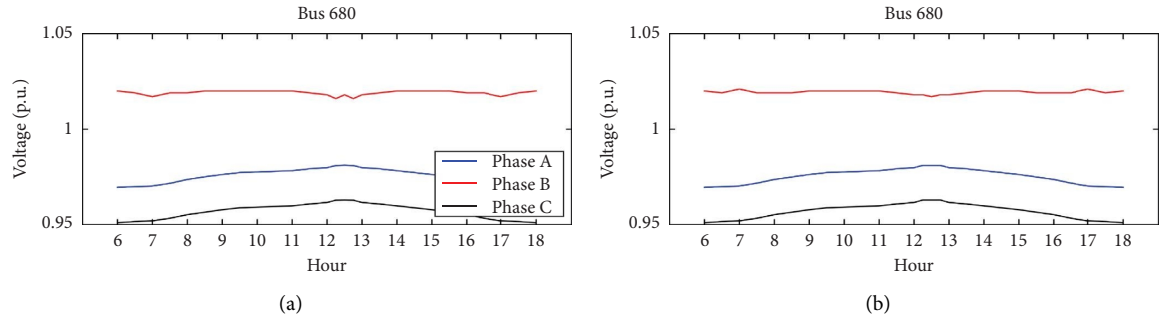

Figure 16: Bus voltages with control on PV inverters for +10% load change. (a) VVC control. (b) VWC control.

5. Bus Voltage Analysis Using Real-Time Simulation

The study is further extended with an unbalanced DN (IEEE-13 bus network) developed in RTDS, having the constant load at buses 634, 645, and 671 and PV integrated at buses 634, 671, and 680 (Figure 1). However, in this study, hourly sampled data on solar radiation are considered (Figure 2(b)) to reduce the burden in real-time simulation. The voltage analysis is performed for two cases such as without PHIL and with PHIL resources integrated at one of the buses in the network.

Table 1: Change in power; S (kVA), P (kW), and Q (kVAR) supplied by the grid with changes in system loads.

Load condition/grid power	With VVC			With VWC		
	P	Q	S	P	Q	S
Base load	2449.0	3043.0	3906.0	2447.0	3037.0	3900.0
+5% increment at all	2539.0	3109.0	4014.0	2531.0	3101.0	4002.0
+10% increment at all	2629.0	3177.0	4123.0	2629.0	3176.0	4123.0
−5% increment at all	2359.0	2975.0	3797.0	2361.0	2974.0	3797.0
−10% increment at all	2268.0	2909.0	3688.0	2256.0	2910.0	3682.0
+5% at bus 671 and −10% at bus 634	2468.0	3051.0	3924.0	2468.0	3050.0	3924.0

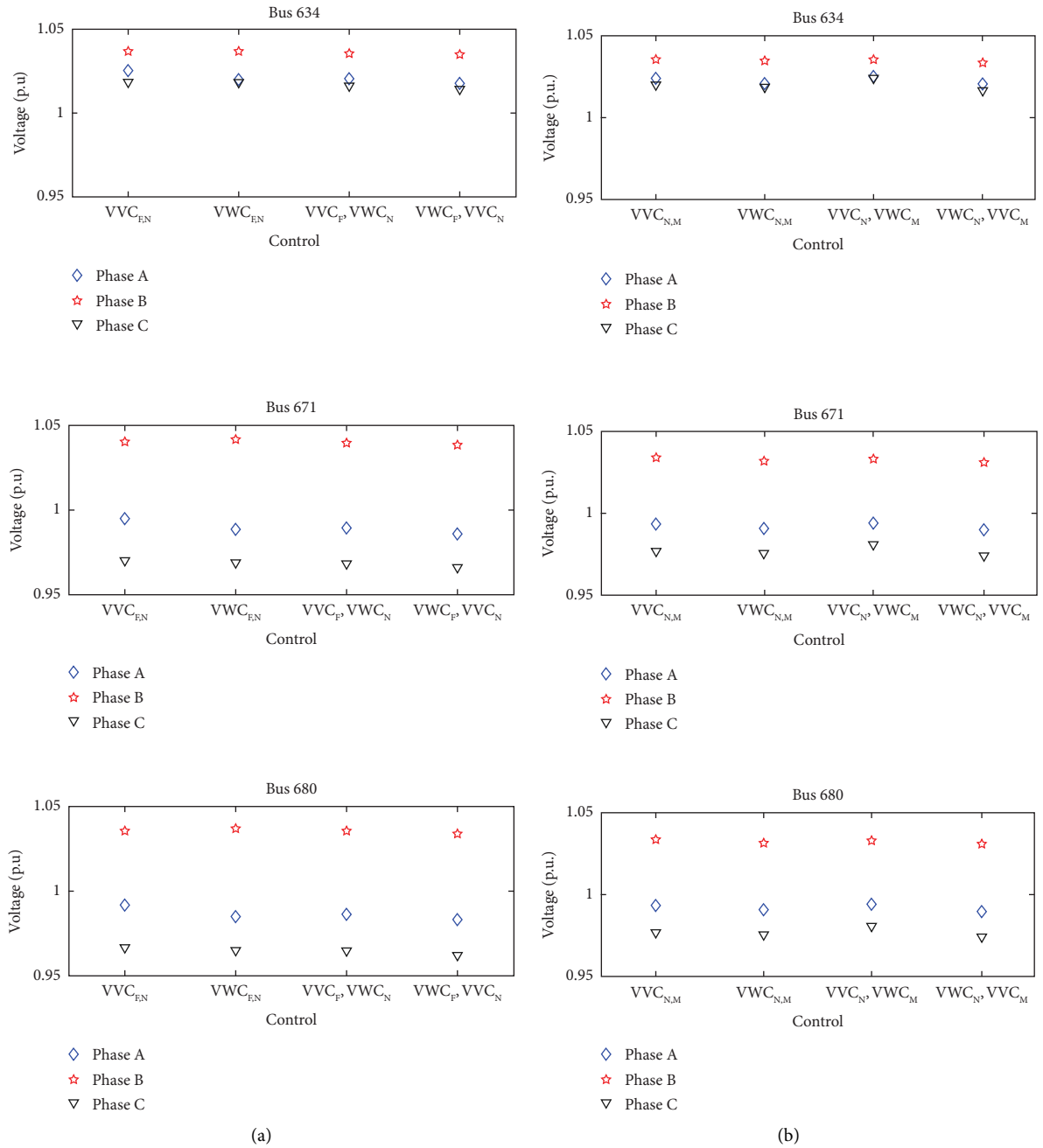

Figure 17: Bus voltages and PVs power with control on PV inverters and PHIL. (a) PHIL at bus 671. (b) PHIL at bus 680.

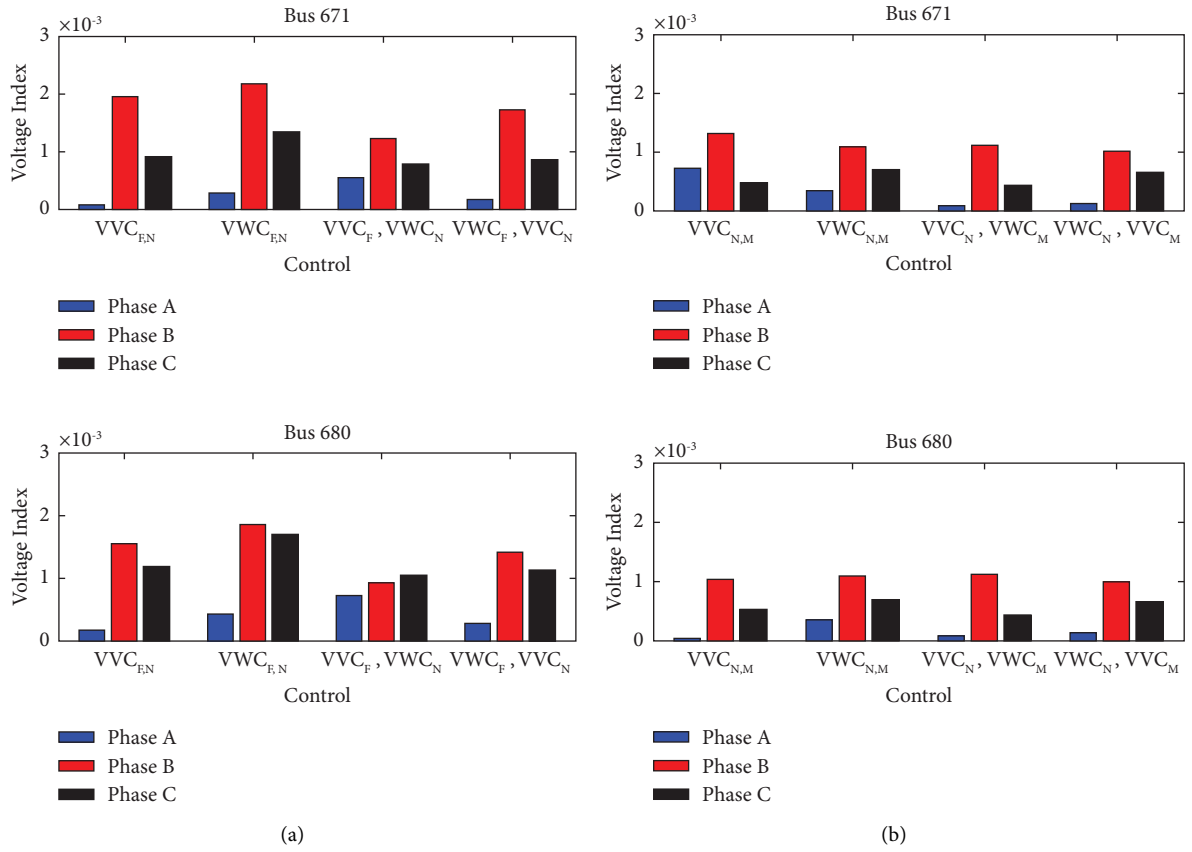

Figure 18: Voltage index with control on PV inverters and PHIL. (a) PHIL on bus 671. (b) PHIL on bus 680.

5.1. Bus Voltage Analysis without PHIL. Two solar radiation profiles (Figure 2(b)) such as SR_1 reaches as high as 1140 W/m^2 at 12:30 pm, responsible for voltage violation (as discussed later) while SR_2 has a peak of 1000 W/m^2 and is considered for PV power generation. At base load conditions, the voltage profile without any control implemented on PV inverters is shown in Figure 14. As indicated, a voltage violation is observed at 12:30 hrs with power generation from solar radiation SR_1. Further, note that over-voltage violation does not exist for phase B at bus 671. On the other hand, even without control of the PV inverter, the voltage variation remains within limits for PV generation from solar radiation SR_2. Further study, based on the control algorithm is discussed only for radiation SR_1.

Having implemented the proposed VVC and VWC control algorithms, real-time simulation results are shown in Figure 15. Here, the active power injected by all three PVs is the same for both the control algorithms, and the voltage profile at feeder buses for VVC is more stable compare to VWC. An under-voltage (beyond the limit) is observed at feeder end bus 671, using VWC, because more power is curtailed.

The impact of VVC and VWC at a 10% increment with respect to base load is presented in Figure 16. As load increases by 10%, the power supplied by the grid increases, while the voltage at the feeder end drops but remains within limits. It can be observed that at 12:30 hrs, the voltage of phases A and C increases, while a small drop is observed in phase B voltage at this time instant.

Table 1 presents the power changes in the network for different load conditions: base load, +5%, +10%, −5%, and −10% at all bus loads, and +5% of bus 671 with −10% of bus 634. From the table, it is observed that after applying the control, the grid power supplied to the network has increased (decreased) with an increase (decrease) in the load. Further, the grid power supplied via VWC remains lower as compared to the power supplied with VVC.

5.2. Bus Voltage with PHIL. Next, the voltage analysis is performed for PHIL placement at one of the buses. The power flow from PHIL is performed using droop control. In the study, however, PV inverters implemented in RTDS are controlled via either VVC, VWC, or a combination of VVC-VWC. The combinations of these control functions are carried out at different locations. These nodes are referred to as *N*, *M*, and *F* corresponding to bus 634 (near to the grid), bus 671 (mid the grid), and bus 680 (far from the grid), respectively (Figure 1).

As shown in Figure 17, the *x*-axis represents the control methods such as VVC and VWC with subscripts corresponding to locations, *N*, *M*, and *F* in the network, being implemented on PV inverters. As in Figure 17(a), having PHIL placed on bus 671 (mid-grid with three-phase load), the voltage margin among the phases is closest at bus 634, while this increases at bus 671 and 680. The use of control methods, VVC, VWC, or their combination does not have any impact on the voltage status of the buses. Similarly, having PHIL at

bus 680 as indicated in Figure 17(b) does not seem to cause any significant changes in the voltage status at bus 634 for different control methods. Comparatively, at bus 671 and 680, the voltage margin among the phases is observed to get reduced, i.e., improved. Here, it can be concluded that the placement of droop-controlled PV (PHIL) on bus 680 (feeder end bus) would be better than bus 671 (mid-grid).

The above discussion is further supported by the calculation of the voltage index, $V_{n,\phi}^{\text{index}}$ to quantify the voltage variation throughout the network, which is given as follows:

$$V_{n,\phi}^{\text{index}} = \sum_{i=1}^{t} \left(1 - \left|V_{n,\phi}\right|\right)^2. \tag{13}$$

The maximum and minimum voltage limit at every bus is set as $v^{\min} = 0.95$ p.u. and $v^{\max} = 1.05$ p.u. As shown in Figure 18, the voltage index for PHIL placed on bus 680 is less compared to PHIL placement on bus 671 because bus 680 is a feeder end bus without any load connected.

6. Conclusions

The study presented a detailed analysis of voltage distribution in an unbalanced DN, with the implementation of an update of VVC/VWC based on estimated voltage sensitivity from local measurement bus data. The voltage status in the network remained within limits for PV power generation due to transient varying at the time of minimum load demand. The dip in voltage was more severely caused by load surge rather than transient varying solar radiation. The real-time simulation suggested overvoltage due to a surge in solar radiation without control, even for a short time. This was, however, mitigated with regulated reactive power from PV inverters using the proposed approach. The bus voltage could be regulated within $[1.05 - 0.95]$ p.u. The results obtained on the addition of PHIL at one of the buses reinforced the verification of the proposed control approach in the mitigation of voltage problems on real solar radiation profiles. Compared with existing works, the proposed control approach does not use communication links and is thus more reliable.

Data Availability

The data used to support the findings of this study are included within the article.

Conflicts of Interest

The authors declare that they have no conflicts of interest.

Acknowledgments

The part of the study presented on PHIL has been performed using the ERIGrid 2.0 Research Infrastructure and is part of a project that has received funding from the European Union's Horizon 2020 Research and Innovation Programme under the grant Agreement no. 870620. The support of the European Research Infrastructure ERIGrid 2.0 and its partner VTT is very much appreciated.

References

[1] M. Ahmadi, M. E. Lotfy, R. Shigenobu, A. Yona, and T. Senjyu, "Optimal sizing and placement of rooftop solar photovoltaic at Kabul city real distribution network," *IET Generation, Transmission and Distribution*, vol. 12, no. 2, pp. 303–309, 2018.

[2] M. Bazrafshan and N. Gatsis, "Decentralized stochastic optimal power flow in radial networks with distributed generation," *IEEE Transactions on Smart Grid*, vol. 8, no. 2, pp. 787–801, 2017.

[3] Q. Xie, H. Hui, Y. Ding et al., "Use of demand response for voltage regulation in power distribution systems with flexible resources," *IET Generation, Transmission and Distribution*, vol. 14, no. 5, pp. 883–892, 2020.

[4] H. U. Habib, A. Waqar, S. Sohail et al., "Optimal placement and sizing problem for power loss minimization and voltage profile improvement of distribution networks under seasonal loads using Harris hawks optimizer," *International Transactions on Electrical Energy Systems*, vol. 2022, Article ID 8640423, 49 pages, 2022.

[5] M. Emmanuel, J. Giraldez, P. Gotseff, and A. Hoke, "Estimation of solar photovoltaic energy curtailment due to volt–watt control," *IET Renewable Power Generation*, vol. 14, no. 4, pp. 640–646, 2020.

[6] A. O'Connell and A. Keane, "Volt–var curves for photovoltaic inverters in distribution systems," *IET Generation, Transmission and Distribution*, vol. 11, no. 3, pp. 730–739, 2017.

[7] N. Li, G. Qu, and M. Dahleh, "Real-time decentralized voltage control in distribution networks," in *Proceeding Allerton Conference Communication Control Computation*, pp. 582–588, Allerton, IL, USA, October 2014.

[8] A. Inaolaji, A. Savasci, and S. Paudyal, "Distribution grid optimal power flow in unbalanced multiphase networks with volt-var and volt-watt droop settings of smart inverters," *IEEE Transactions on Industry Applications*, vol. 58, no. 5, pp. 5832–5843, 2022.

[9] J. Seuss, M. J. Reno, M. Lave, R. J. Broderick, and S. Grijalva, "Advanced inverter controls to dispatch distributed PV systems," in *Proceedings of the IEEE 43rd Photovoltaic Specialists Conference (PVSC)*, pp. 1387–1392, Portland, OR, USA, June 2016.

[10] D. Mendoza Osorio and J. Rosero Garcia, "Optimization of distributed energy resources in distribution networks: applications of convex optimal power flow formulations in distribution networks," *International Transactions on Electrical Energy Systems*, vol. 2023, Article ID 1000512, 16 pages, 2023.

[11] A. Guichi, S. Mekhilef, E. M. Berkouk, and A. Talha, "Optimal control of grid-connected microgrid PV-based source under partially shaded conditions," *Energy*, vol. 230, Article ID 120649, 2021.

[12] S. Chakraborty, A. Hoke, and B. Lundstrom, "Evaluation of multiple inverter volt-var control interactions with realistic grid impedances," in *Proceedings of the IEEE Power Energy Society General Meeting*, pp. 1–5, New York, NY, USA, July 2015.

[13] M. G. Kashani, M. Mobarrez, and S. Bhattacharya, "Smart inverter volt-watt control design in high PV-penetrated distribution systems," *IEEE Transactions on Industry Applications*, vol. 55, no. 2, pp. 1147–1156, 2019.

[14] S. Ahmad, H. Mubarak, U. K. Jhuma, T. Ahmed, S. Mekhilef, and H. Mokhlis, "Point of common coupling voltage modulated direct power control of grid-tied photovoltaic inverter for ac microgrid application," *International Transactions on Electrical Energy Systems*, vol. 2023, Article ID 3641907, 22 pages, 2023.

[15] N. Kumar, G. Singh, and H. Kebede, "An optimized framework of the integrated renewable energy and power quality model for the smart grid," *International Transactions on Electrical Energy Systems*, vol. 2023, Article ID 6769690, 11 pages, 2023.

[16] Y. Wang, N. Zhang, H. Li, J. Yang, and C. Kang, "Linear three-phase power flow for unbalanced active distribution networks with PV nodes," *CSEE Journal of Power and Energy Systems*, vol. 3, no. 3, pp. 321–324, 2017.

[17] Z. Liu, Z. Guo, Q. Chen et al., "A review of data-driven smart building-integrated photovoltaic systems: challenges and objectives," *Energy*, vol. 263, Article ID 126082, 2023.

[18] S. Mahdi Noori Ra, P. Scott, M. Mahmoodi, and A. Attarha, "Data-driven adjustable robust solution to voltage-regulation problem in PV-rich distribution systems," *International Journal of Electrical Power and Energy Systems*, vol. 141, no. 141, Article ID 108118, 2022.

[19] C. Zhang, J. Li, Y. J. Zhang, and Z. Xu, "Optimal location planning of renewable distributed generation units in distribution networks: an analytical approach," *IEEE Transactions on Power Systems*, vol. 33, no. 3, pp. 2742–2753, 2018.

[20] Institute of Electrical and Electronics Engineers, "Ieee 13 bus feeder," 2018, http://images.shoutwiki.com/mindworks/7/7e/IEEE_13_Bus_Power_System.pdf.

[21] Electric Power Research Institute (EPRI), "Opendsswiki," 2018, https://sourceforge.net/p/electricdss/code/HEAD/tree/trunk/Distrib/EPRITestCircuits/.

[22] M. Reno and K. Coogan, "Grid Integrated Distributed PV (GridPV)," Technical Report, Sandia National Laboratories, Albuquerque, NM, USA, 2013.

[23] A. Yadav, N. Kishor, and R. Negi, "Voltage profile analysis in distribution network for allowable hosting capacity from PV integration," in *Proceedings of the 1st International Conference on Sustainable Technology for Power and Energy Systems (STPES)*, Srinagar, India, July 2022.

[24] J. Zhang, Z. Wang, X. Zheng, L. Guan, and C. Y. Chung, "Locally weighted ridge regression for power system online sensitivity identification considering data collinearity," *IEEE Transactions on Power Systems*, vol. 33, no. 2, pp. 1624–1634, 2018.

[25] Sourceforge, "Electricdss discussion," 2018, https://sourceforge.net/p/electricdss/discussion/search/?q=loadshape&limit=50.

[26] Z. Wang, D. S. Kirschen, and B. Zhang, "Accurate semidefinite programming models for optimal power flow in distribution systems," 2017, https://arxiv.org/abs/1711.07853.